

Alma Mater Studiorum Università di Bologna
Archivio istituzionale della ricerca

Influence of Friction Stir Processing on the Microstructure and Mechanical Properties of a compocast AA2024-Al₂O₃ nanocomposite

This is the final peer-reviewed author's accepted manuscript (postprint) of the following publication:

Published Version:

Hoziefa, W., Toschi, S., Ahmed, M.M.Z., Morri Alessandro, A. A. Mahdy, El-Sayed Seleman, M.M., et al. (2016). Influence of Friction Stir Processing on the Microstructure and Mechanical Properties of a compocast AA2024-Al₂O₃ nanocomposite. MATERIALS & DESIGN, 106, 273-284 [10.1016/j.matdes.2016.05.114].

Availability:

This version is available at: <https://hdl.handle.net/11585/541962> since: 2017-05-16

Published:

DOI: <http://doi.org/10.1016/j.matdes.2016.05.114>

Terms of use:

Some rights reserved. The terms and conditions for the reuse of this version of the manuscript are specified in the publishing policy. For all terms of use and more information see the publisher's website.

This item was downloaded from IRIS Università di Bologna (<https://cris.unibo.it/>).
When citing, please refer to the published version.

(Article begins on next page)

This is the final peer-reviewed accepted manuscript of:

W. Hoziefa, S. Toschi, M.M.Z. Ahmed, Al. Morri, A.A. Mahdy, M.M. El-Sayed Seleman, I. El-Mahallawi, L. Ceschini, A. Atlam, ***Influence of friction stir processing on the microstructure and mechanical properties of a compocast AA2024-Al2O3 nanocomposite***, *Materials & Design*, Volume 106, 2016, Pages 273-284, ISSN 0264-1275

The final published version is available online at:

<https://doi.org/10.1016/j.matdes.2016.05.114>

Rights / License:

The terms and conditions for the reuse of this version of the manuscript are specified in the publishing policy. For all terms of use and more information see the publisher's website.

This item was downloaded from IRIS Università di Bologna (<https://cris.unibo.it/>)

When citing, please refer to the published version.

Manuscript Number: JMAD-D-16-02194R1

Title: Influence of Friction Stir Processing on the Microstructure and Mechanical Properties of a compocast AA2024-Al2O3 nanocomposite

Article Type: Research Paper

Keywords: AA2024 alloy; Nanocomposites; Compocasting; Friction Stir Processing.

Corresponding Author: Dr. Stefania Toschi,

Corresponding Author's Institution: University of Bologna

First Author: Wael Hoziefa, PhD

Order of Authors: Wael Hoziefa, PhD; Stefania Toschi; Mohamed Mohamed Zaky Ahmed, Professor; Alessandro Morri, Professor; Amir Mahdy, PhD; Mohamed El-Sayed Seleman, Dr; Iman El-Mahallawi, Professor; Lorella Ceschini, Professor; Ahmed Gomaa Atlam

Abstract: The effect of friction stir processing (FSP) on the microstructure and mechanical properties of a semi-solid cast AA2024-1wt.%Al2O3 nanocomposite was investigated. For comparison, plates of unreinforced AA2024 alloy were also cast and processed at the same FSP conditions (400 rpm, 20mm/min). The microstructure of all the produced materials was investigated using optical microscopy (OM), scanning electron microscopy (SEM) and electron backscattered diffraction (EBSD). Microhardness and tensile tests were carried out on the unreinforced AA2024 alloy and AA2024-Al2O3 nanocomposite before and after FSP. The addition of 1wt% of Al2O3 nanoparticles significantly reduced the grain size of both the cast and FSPed microstructures, leading to a grain size reduction from 28 μm to 18 μm in the cast condition, and from 3.7 μm to 2.7 μm after FSP. The application of FSP to AA2024-Al2O3 nanocomposite enhanced the tensile strength and yield strength by 71% and 30%, respectively, in comparison to the as cast matrix, as a result of the uniform distribution of Al2O3 reinforcement and grain refinement of Al matrix. The combined application of compocasting and FSP resulted to be a promising method to treat casting defects and to produce nanocomposites characterised by good reinforcement dispersion and high strength and ductility.

Influence of Friction Stir Processing on the Microstructure and Mechanical Properties of a compocast AA2024-Al₂O₃ nanocomposite

W. Hoziefa^a, S. Toschi^b, M.M.Z. Ahmed^{c,d}, Al. Morri^b, A. A. Mahdy^a,

M.M. El-Sayed Seleman^{c,d}, I. El-Mahallawi^e, L. Ceschini^b, A. Atlam^a.

^a Department of Metallurgy, Mining & Petroleum Engineering, Faculty of Engineering, Al-Azhar University, P.O. Box 11884, Cairo, Egypt.

^b Department of Industrial Engineering (DIN), Alma Mater Studiorum, University of Bologna, Viale Risorgimento 4, 40136 Bologna, Italy.

^c Department of Metallurgical and Materials Engineering, Faculty of Petroleum and Mining Engineering, Suez University, P.O. Box 43721, Suez, Egypt.

^d Suez and Sinai Metallurgical and Materials Research Center of Scientific Excellence (SSMMR-CSE), Suez University, Suez, Egypt.

^e Department of Metallurgy and Materials Engineering, Faculty of Engineering, Cairo University, 12316 Giza, Egypt.

Corresponding author: Dr Stefania Toschi

E-mail: stefania.toschi3@unibo.it

Tel.: +39 051 2093142

Fax: +39 051 2093467

Influence of Friction Stir Processing on the Microstructure and Mechanical Properties of a compocast AA2024-Al₂O₃ nanocomposite

**W. Hoziefa^a, S. Toschi^b, M.M.Z. Ahmed^{c,d}, Al. Morri^b, A. A. Mahdy^a,
M.M. El-Sayed Seleman^{c,d}, I. El-Mahallawi^e, L. Ceschini^b, A. Atlam^a.**

^a Department of Metallurgy, Mining & Petroleum Engineering, Faculty of Engineering, Al-Azhar University, P.O. Box 11884, Cairo, Egypt.

^b Department of Industrial Engineering (DIN), Alma Mater Studiorum, University of Bologna, Viale Risorgimento 4, 40136 Bologna, Italy.

^c Department of Metallurgical and Materials Engineering, Faculty of Petroleum and Mining Engineering, Suez University, P.O. Box 43721, Suez, Egypt.

^d Suez and Sinai Metallurgical and Materials Research Center of Scientific Excellence (SSMMR-CSE), Suez University, Suez, Egypt.

^e Department of Metallurgy and Materials Engineering, Faculty of Engineering, Cairo University, 12316 Giza, Egypt.

Abstract. The effect of friction stir processing (FSP) on the microstructure and mechanical properties of a semi-solid cast AA2024-1wt.% Al₂O₃ nanocomposite was investigated. For comparison, plates of unreinforced AA2024 alloy were also cast and processed at the same FSP conditions (400 rpm, 20mm/min). The microstructure of all the produced materials was investigated using optical microscopy (OM), scanning electron microscopy (SEM) and electron backscattered diffraction (EBSD). Microhardness and tensile tests were carried out on the unreinforced AA2024 alloy and AA2024-Al₂O₃ nanocomposite before and after FSP. The addition of 1wt% of Al₂O₃ nanoparticles significantly reduced the grain size of both the cast and FSPed microstructures, leading to a grain size reduction from 28 µm to 18 µm in the cast condition, and from 3.7 µm to 2.7 µm after FSP. The application of FSP to AA2024-Al₂O₃ nanocomposite enhanced the tensile strength and yield strength by 71% and 30%, respectively, in comparison to the as cast matrix, as a result of the uniform distribution of Al₂O₃ reinforcement and grain refinement of Al matrix. The combined application of compocasting and FSP resulted to be a promising method to treat casting defects and to produce nanocomposites characterised by good reinforcement dispersion and high strength and ductility.

Keywords: AA2024 Al alloy, Nanocomposites, Compocasting, Friction Stir Processing.

1. Introduction

Aluminium matrix nanocomposites (Al-MNCs), characterised by reinforcing particles smaller than 100 nm, offer significant opportunities as structural materials, since they present enhanced mechanical properties in comparison to unreinforced matrix and microcomposites (Al-MCs) [1].

Liquid state processing of Al-based nanocomposites is strongly limited by the low wettability of ceramic nanoparticles into the molten metal; as a result, although they would enable the production of complex shape parts, traditional liquid routes such as casting are usually associated with particle clustering, high amounts of casting defects related to the addition of nanoparticles and particle segregation induced by the different specific gravity of the matrix and reinforcement [2, 3].

Semisolid casting has been proposed as a possible production route to overcome such problems, by improving nanoparticle wettability due to the higher viscosity of the semi-solid matrix in comparison to the liquid state, which would also help facilitating the mechanical entrapment of the reinforcing phase [4, 5]. The addition of reinforcing particles to the matrix at the semi-solid state in association with mechanical stirring is usually referred to as compocasting.

Al-based composites reinforced with Al_2O_3 nanoparticles were produced through the semi-solid casting route by El-Mahallawi *et al.* [6, 7], who reported an enhancement of both tensile strength and elongation to failure associated with a refined structure in comparison to the unreinforced alloy. Although casting defects are reduced by semi-solid casting in comparison to liquid state routes, the presence of porosities and cavities associated with nanoparticles are however reported [6, 7]. Zhou *et al.* [8] showed that wettability cannot be enhanced by simple mechanical stirring; in this regard, the authors reported that breaking the gas layer surrounding the particles would be necessary to improve particle wettability.

Al based nanocomposites have also been investigated as surface materials, aiming to exploit their mechanical properties and hardness to produce components with superior wear resistance. For this purpose, secondary processes are currently being investigated to obtain an even distribution of particles, usually difficult to be achieved by conventional surface treatments [9]. Friction-stir processing (FSP), an innovative thermo-mechanical processing technique adapted from the concept of friction stir welding, has recently been proposed to this aim [10–11]. The process is known to induce microstructural homogenisation, grain refinement and improved static properties in Al alloys [12–17]. Guo *et al.* used FSP to fabricate Al-based nanocomposites and studied the effects of the nano- Al_2O_3 particle addition on grain structure and mechanical properties [18]. They reported that the pinning effect of Al_2O_3 particles retarded grain growth following recrystallization during FSP

and led to a more pronounced reduction in grain size [18]. Gandra *et al.* used FSP to develop aluminium based functionally graded MMCs and examined the effect of overlapping direction on the surface and thickness layer [19-21]. Overlapping by the retreating side was found to generate smoother surfaces, while overlapping by the advancing side led to more uniform thickness layers. In their study of wear behaviour of functionally graded MMCs the authors reported a reduction of wear rate by about 13% after an increase of about 30% in the hardness [21].

Developing new routes for the manufacturing of metal matrix composites (MMCs) is of considerable importance. These new routes are based on the combination of the conventional liquid state techniques and friction stir processing [22-25]. In situ mixed salt methods were used to fabricate aluminium MMCs that were subsequently processed by FSP to improve the distribution of reinforcing particles [22-24]. Recently, Ma *et al.* studied the microstructure and mechanical properties of in-situ nanosized $\text{TiB}_2/\text{Al-Mg-Si}$ composites processed by friction stir processing [22]. They reported that the initial unprocessed composite had a grain size of 50–100 μm with the synthesized nanosized TiB_2 particles almost agglomerated to micrometric clusters at grain boundaries. Comparatively, after FSP, the nugget zone was characterized by fine and equiaxed recrystallized grains (1–5 μm in average grain size). The initial clusters were also broken up, while the nanosized TiB_2 particles were distributed much more uniformly in the matrix, acting as effective pins to interact with dislocations [22]. Also Chen *et al.* [23] studied the effects of nano particles on the microstructural evolution of FSPed in-situ $\text{TiB}_2/6063\text{Al}$ composite. They observed homogenous redistribution of nanosized TiB_2 particles in a fine-grained in-situ AA6063/ TiB_2 composite through FSP. More recently, Zhao *et al.* [24] investigated the effect of FSP on the microstructure and superplasticity of in situ nano- $\text{ZrB}_2/2024\text{Al}$ composites. FSP resulted in grain refining of the cast structure and in the more even distribution of nanoparticles [24]. The effect of multipass FSP on the microstructure and mechanical properties of $\text{Al}_3\text{Ti}/\text{A356}$ composites was examined by Yang *et al.* [25], who found that after multi-pass FSP, both the strength and ductility of the composite samples were gradually enhanced [25].

The present study is intended to investigate the possibility to produce a AA2024-based composite containing Al_2O_3 nanoparticles, by combining compocasting technique and FSP. The aim is also extended to evaluate the effect of FSP, performed at fixed processing parameters, on the microstructural and mechanical properties of the produced composite.

2. Materials and methods

AA2024-Al₂O₃ nanocomposite was produced by adding 1 wt% of Al₂O₃ nanoparticles into AA2024 Al matrix at the semi-solid state through mechanical stirring. For comparison, the unreinforced AA2024 alloy was fabricated at the same conditions. The chemical composition of the matrix alloy and the properties of the reinforcing particles are reported in Tables 1 and 2, respectively.

The compocasting process for the unreinforced matrix alloy and its nanocomposite plates was carried out in a furnace designed for this work. The apparatus consists of a lift out graphite crucible with a maximum capacity of 500 g and a controlling heating system, provided with a stirring unit. Al₂O₃ nanoparticles were milled by high energy ball milling at 200 rpm for 2 min. in order to preliminarily eliminate particle clusters. Al₂O₃ nanoparticles were then wrapped in an aluminium foil and preheated at 200°C for 2 h. A charge of 400 g of the matrix alloy was introduced into the crucible and heated up to 700°C. The molten alloy was then degassed with hexachlorethane degasser tablets. After the degassing process, the pre-heated Al₂O₃ packages were simultaneously added to the matrix at 610°C, while mechanical stirring was applied for 1 min at 800 rpm. The amount of Al₂O₃ nanoparticles was added to achieve 1 wt % of the produced casting. The unreinforced alloy and the composite were then cast in a stainless steel mould 250 mm long, 50mm wide and 10 mm thick.

Friction Stir Processing (FSP) was then applied to the cast plates of the unreinforced alloy and nanocomposite. A H13 steel tool was used for sample processing (dimensions of the cylindrical tool: pin diameter 6 mm, pin length 6 mm and shoulder diameter 20 mm). A single FSP pass was performed at a rotation rate of 400 rpm, linear speed of 20 mm/min, plunge depth of 6 mm and tool tilt angle of 3°. Macrographs of the cast AA2024-Al₂O₃ nanocomposite plate before and after FSP are shown in Fig. 1.

For microstructural analyses, samples were cross sectioned perpendicular to the processing direction and polished according to the standard techniques for examination by optical microscopy (OM), multifocal microscopy (MM), scanning electron microscopy (SEM) equipped with energy dispersive spectroscopy (EDS) and electron backscattered diffraction (EBSD) systems. All the samples after final mechanical polishing were etched with Keller's etchant to be examined by OM, MM and SEM. Samples for EBSD analyses were electro-polished with a solution of 30% nitric acid in methanol for 20 s at 14 V and -15°C. The EBSD samples were then mechanically polished with colloidal nanoSiO₂ for a few seconds to remove any second phase particles from the surface. The EBSD analyses were conducted using Quanta FEG 250 SEM equipped with Hikari EDAX EBSD

camera controlled by TEAM software, using 1 μm step size for the as cast materials and 0.5 μm step size for the FSPed materials. EBSD data were collected for grain structure and microstructural analyses. The data were subjected to standard clean-up procedures involving grain tolerance angle of 5° and a minimum grain size of 4 pixels for grain boundary, misorientation angle distribution and texture analysis.

Density of the produced materials was determined, based on Archimedes' principle through an analytical balance (precision $\pm 0.0001\text{ g}$) on representative samples ($5 \times 5 \times 5 \text{ mm}^3$). Vickers microhardness profiles were performed on the cross sections of the FSPed samples, under a 4.9 N load and for a dwell time of 10s. Twenty microhardness indentations were performed every 0.5 mm at a different depth from the FSP surface, namely 0.5, 2.5 and 5 mm, as shown in Fig. 2a. For comparison, microhardness of the as cast matrix and nanocomposite was measured at the same manner, taking the average of five micro-Vickers indentations. Flat tensile specimens with a gauge length of 25 mm and a section of $3 \times 6\text{ mm}$ (according to ISO6892-1) were cut along the FSP direction of the plates, aiming to have the entire gauge section in the FSPed zone (Fig. 2b,c). Three tensile specimens for each material, both in the as-cast condition and after FSP (as shown in Table 3), were tested using an electromechanical testing machine. Fracture surfaces were analysed thoroughly using both MM and SEM-EDS.

3. Results and Discussion

3.1 Macro- and Microstructural analysis

Figure 3 shows MM images of the macrostructure of the unreinforced alloy and nanocomposite in the as-cast condition. From these images it is obvious that in comparison to the unreinforced alloy (Fig. 3a), the AA2024- Al_2O_3 nanocomposite (Fig. 3b) is characterised by a dense population of circular pores, mainly located in the central zone of the sample. The presence of pores in the semi-solid processed composite was expected, as widely reported by several investigators [3–5]. Wettability issues associated with the addition of ceramic nanoparticles as well as air entrapment related to particle clustering during the stirring process are in fact known to induce the formation of casting defects, both in liquid and semisolid state processed Al-based nanocomposites [6–7]. Thereto, the obtained results, showing the formation of pores as a consequence of nanoparticles addition during the compocasting process, are consistent with the findings of other authors [5-7].

Optical micrographs of the as-cast unreinforced alloy and nanocomposite are shown in Figs. 4 and 5, respectively. The microstructures of both as-cast materials is characterized by the presence of α -Al dendritic structure surrounded by eutectic structure. Due to the semi-solid processing, the α -dendrites are characterised by a slightly pronounced quasi-globular morphology (Figs 4b, 5b). The composition of interdendritic intermetallic particles was investigated through SEM-EDS (Fig. 4c). The analysis shows the presence of binary and ternary particles containing Al, Cu and Mg, probably the Al_2Cu and Al_2CuMg phases. No difference in the chemical composition of coarse intermetallic particles was detected by SEM between the alloy matrix and the composite. SEM analyses carried out on the nanocomposite confirmed the relationship between porosities and nanoparticles. The internal surfaces of the pores, in fact, showed the presence of Al_2O_3 clusters, which probably induced their formation (Fig. 5c,d). Nevertheless, small Al_2O_3 clusters were also found in the interdendritic regions, as a result of the force exerted by the advancing solidification front (Fig. 5c,e).

Macrographs of the FSPed unreinforced alloy and nanocomposite are showed in Fig. 6a and b, respectively. The processed zones of both materials are characterised by different nugget zone (NZ)-Thermomechanical affected zone (TMAZ) interface between the advancing side (AS) and retreating side (RS): while a sharp and defined border is observed at the AS, a more diffuse interface is found at the RS. This behaviour has been previously reported by other authors [10] and should be related to the material plastic flow around the pin during the tool translation and rotation. As a consequence of rotation, the material is swept from the AS to the RS, where it is accumulated. This results in the formation of a transition zone at the RS and a well-defined border at the AS.

It can be observed that the FSP significantly reduced the content of porosities associated with the Al_2O_3 nanoparticles, as highlighted in Fig. 6b. This is due to the thermomechanical action of the pin, which induces plastic deformation of the matrix, therefore eliminating voids and cavities, as also observed by different authors, also contributing to enhanced nanoparticles dispersion inside the nugget zone [15, 16, 19, 20, 26]. The beneficial effect of FSP on casting defects was confirmed by density measurements, whose results are shown in Fig. 7.

Figs. 8 and 9 show optical images of the FSPed AA2024 alloy and AA2024- Al_2O_3 nanocomposite, respectively. By comparing images of the base material and the nugget zone (Figs. 8-9, a and f), it is clear that the FSP induced a significant grain refinement in both the materials, as a result of the FSP induced recrystallization processes [10, 11]. Elongated structures were found in the TMAZ, as a result of material flow induced by the pin. As a confirmation of the previous observations, both the FSPed unreinforced alloy and nanocomposite presented a well-defined boundary at the advancing side between NZ and TMAZ, while no clear distinction was observed at the retreating side (Figs. 8-9, b and d).

SEM-EDS images of the FSPed samples are presented in Fig. 10. A very fine grained microstructure, due to the dynamic recrystallization process occurring during FSP, was observed in the NZ of both the unreinforced alloy and nanocomposite. As a consequence of the pin action, the size and the aspect ratio of the intermetallic phases decreased significantly after FSP, as seen in Fig 10a,b. This can be mainly related to the mechanical fragmentation, but also to the elevated temperature induced by the pin rotation, which could have partially dissolved the intermetallic particles [10, 11]. Al_2O_3 clusters were identified in the nanocomposite base material, mostly in the interdendritic areas (Fig. 10d); on the contrary, no appreciable particle agglomeration was detected by SEM in the NZ (Fig. 10c). It is therefore inferred that FSP, by inducing localised severe plastic deformation, may have enhanced the nanoparticle distribution within the NZ.

3.2 Grain structure and texture characterized using EBSD

Aiming to compare the grain structure before and after FSP, EBSD maps were acquired using $1\mu\text{m}$ step size in the as cast materials and using $0.5\mu\text{m}$ step size inside the NG zone of the FSPed materials. The orientation image (OIM) maps as obtained in inverse pole figure coloring (IPF) for the as cast and FSPed materials without and with Al_2O_3 nanoparticles are illustrated in Fig. 11a,b,c and d, respectively. The OIM maps of the as cast materials (Fig. 11a,b) consist of coarse grain structure, dominated by near blue $\langle 111 \rangle$ orientation. It can be observed that the particles on the grain boundaries resulted in poor indexing, while high indexing ($>90\%$) was obtained inside the

grains. A similar observation is noted by Ma *et al.* [22] in their EBSD investigation of nanosized TiB₂ reinforced aluminum. The average grain size of the as cast alloy without nanoparticles is about 28 μm while that of the as cast nanocomposite is about 18 μm . This can be attributed to the effect of nanoparticle addition, that enhanced the heterogeneous nucleation and resulted in relatively finer grain structure.

FSP, as a severe plastic deformation process, resulted in significant grain refining in the NG zone. It has been reported that the mechanism of grain formation during FSP is mainly continuous and geometric dynamic recrystallization [27]. Ahmed *et al.* [27] compared the grain structure of FSPed aluminum and high strain torsion tested aluminum at strain rate of 15 s⁻¹ up to 9 equivalent strain and reported that this amount of strain resulted in a grain structure similar to that formed in the NG zone of FSPed aluminum. In the OIM maps of the FSPed materials some black areas, representing the poor indexed areas, were found. The cause of this can be explained since during the preparation for EBSD analyses, the samples were mechanically polished after electro-polishing to remove the particles coming up from the sample surface, causing shadowing and significant indexing decrease [28]. As a result, the non-indexed areas on the maps after FSP (Fig. 11 c,d) represent the places of the removed particles upon mechanical polishing. In the FSPed alloy without nanoparticles, such non-indexed areas correspond to intermetallic particles that formed at the grain boundaries during casting that underwent fragmentation due the stirring action during FSP. The amount of black areas increased in the FSPed nanocomposite; this can be due to the presence of both second intermetallic phases and some small nanoparticle clusters. The average grain size of the FSPed unreinforced alloy is about 3.7 μm , while that of the FSPed nanocomposite is about 2.3 μm . The grain size distribution of the FSPed materials is illustrated in Fig. 11e, while the comparison of all the investigated materials, before and after FSP, is depicted in Fig. 11f. The significant grain size reduction after FSP is clearly observed. As a result of the present investigation, the addition of nanoparticles resulted in a reduction of about 50% in the grain size, either in the as cast and the FSPed materials. This finding is similar to the results obtained by Ma *et al.* [22] after FSP of nanosized TiB₂ reinforced aluminum.

Fig. 12a shows the grain boundary map with high angle boundaries >15° in black line and low angle boundaries 5-15° in red line, after the application of suitable EBSD datasets treatment in the FSPed materials. The corresponding misorientation angle distribution is illustrated in Fig. 12b, while Fig. 12c reports the corresponding 111, 101 pole figures, illustrated with respect to the standard shear reference axes (θ , z , r) after the alignment of the friction stir processing axes (WD, TD, ND) with the shear reference frame according to the methodology described elsewhere [29]. The grain

boundary maps show the existence of a significant amount of low angle boundaries as a result of the dynamic recrystallization processes; a larger number of relatively coarse grains can be observed in the unreinforced FSPed alloy in comparison to the FSPed nanocomposite. The misorientation angle distribution is the typical one of recrystallized materials with high number frequency in the FSPed composite, due to the finer grain structure. In terms of texture, it can be noted that the PFs show the typical simple shear texture with B and B- components that were previously reported in friction stir processed/welded aluminum [27,29-30].

3.3 Mechanical properties

Tensile tests and microhardness profiles were carried out on specimens of the unreinforced alloy and nanocomposite, both in the as-cast condition and after friction stir processing.

3.3.1 Microhardness

Microhardness profiles of the FSPed unreinforced alloy and nanocomposite are illustrated in Fig. 13. Trends and data scatter are the result of several superimposed FSP effects on microstructure: nucleation, growth, dispersion of nano-ceramic reinforcement, matrix grain size, dislocation density, dissolution and distribution of precipitates [7, 10, 14]. The reference average microhardness values measured on the base material of unreinforced alloy (82 ± 2 HV_{0.5}) and nanocomposite (101 ± 11 HV_{0.5}) are plotted as a benchmark in Fig. 13. As indicated in Fig. 13a,b,c, a remarkable increase in microhardness was observed in the FSPed nanocomposite compared to the FSPed unreinforced alloy at all the investigated depths. The difference between the unreinforced alloy and the nanocomposite, both in the as cast and in the FSPed conditions, should be ascribed to the strengthening role exerted by nanoparticles and to the grain refinement induced by FSP. Moreover, the increase in microhardness of the FSPed nanocomposite over the reference value (i.e. base material) should be related to the good dispersion of nanoparticles through the FSP.

The higher hardness in the NZ and TMAZ observed in the 0.5 and 2.5 mm depth profiles of the unreinforced alloy compared to the reference value, resulted from the smaller grain size but probably also to precipitation hardening phenomena. High temperatures reached during the FSP, in fact, can partially dissolve Cu based compounds, leading to a subsequent natural age hardening. This effect is less pronounced in the TMAZ, where lower temperatures do not always allow compound dissolution; on the other hand, they could lead to the growth of hardening precipitates with a consequent hardness reduction.

The NZ of the FSPed material shows low hardness data scatter; only in the TMAZ were some peaks registered, which is likely to be due to different local amount of plastic deformation and/or nano-reinforcement distribution. No significant hardness increase compared to the as-cast condition was seen in the deepest profile from the FSPed surface (i.e. 5 mm); in this area, the lower temperature reached can only lead to coarsening of precipitates and this can overtake the strengthening effects of grain refinement for the unreinforced alloy and balance grain refinement and nano-reinforcement for the nanocomposite. It is worth noting that, the alloy and nanocomposites are not heat treated and consequently the hardness profiles have different trends compared to that reported in previous works on heat treated Al alloys [14, 15].

3.3.2 Tensile properties

The results of tensile tests on the investigated materials are presented in Fig. 14. By comparing the tensile properties of as cast matrix and nanocomposite, (Fig. 14a), it is clear that the addition of nanoparticles by simple mechanical stirring at the semi-solid state is not beneficial for tensile properties. In fact, as a result of nanoparticle agglomeration and the associated porosities, a decrease of about 70% in the ultimate tensile strength (UTS) was observed, together with a lower elongation to failure (0.3%). Particle clustering during casting processes is widely reported in the literature to have an adverse effect on mechanical properties and ductility, inducing loss of microstructural cohesion [2–9].

After FSP, a noticeable enhancement of tensile properties in terms of YS (+25%) and UTS (+52%) was observed in the unreinforced alloy compared to the cast condition (Fig. 14a). The positive effect of FSP is due to the refining action of microstructure induced not only by the recrystallization mechanisms associated with the process, but also to the elimination of casting defects (porosities and shrinkage cavities). Elongation to failure, being strongly influenced by the grain size and casting defects as well, increased about ten times in comparison to the unprocessed alloy (7.4% vs. 0.7%, respectively).

FSP applied to the nanocomposite led to an increase in both YS and UTS, with a more consistent enhancement of UTS, in comparison to the FSPed unreinforced alloy (Fig. 14a). This enhancement should be related to the presence of Al_2O_3 nanoparticles, since the samples were processed with the same parameters. As previously observed, FSP processing enabled the elimination of casting defects associated with the addition of nanoparticles, therefore leading to a strong increase of E% in comparison to the cast nanocomposite (7.2% vs 0.3%, respectively).

3.3.3 Fractographic analyses

Multifocal and SEM images of fracture surfaces of the as-cast and the FSPed materials after tensile testing are presented in Figs. 15-16. The low elongation to failure of the unreinforced and unprocessed AA2024 alloy was related to the presence of oxide films on the fracture surfaces (Fig. 15a) and, mainly, to the lack of matrix continuity associated with shrinkage cavities observed by SEM images (Fig. 15b). It is well known that the presence of such defects strongly limits the capacity of plastic deformation of the matrix, with a consequent decrease in the elongation to failure [31]. As a result, the alloy behaves like a brittle material; dimples were in fact not observed.

Al₂O₃ macro-clusters and associated porosities were observed on the fracture surfaces of the as-cast nanocomposite (Fig. 16a), due to the difficulties in obtaining an even distribution of nanoparticles by mechanical stirring of the composite slurry at the semi-solid state. The concurrent presence of oxides, interdendritic cavities and macroscopic particle clusters led to very low elongation to failure (0.3%). Also in this case, the fracture morphology was mainly brittle.

Some oxide films were still present on the fracture surface of FSPed samples (Fig. 15d, 16d); it is inferred that not all the oxides were fragmented and eliminated by the pin rotation. FSP induced completely different fracture morphologies: both the unreinforced alloy and the nanocomposite presented a refined microstructure, characterised by very small and regular dimples, typical of ductile fracture (Fig. 15e,f). Elongation to failure, in fact, strongly increased from the as-cast to the FSP condition. Moreover, in the FSPed nanocomposite (Fig. 16), thanks to the mechanical stirring effect induced by the pin, no significant nanoparticle clustering was observed on the fracture surfaces.

4. Conclusions.

In this research, the feasibility of adding nano-sized Al₂O₃ particles into AA2024 Al alloy through a compocasting technique followed by FSP was investigated. Based on the present study, the following conclusions can be drawn:

- AA2024 Al alloy based composite containing Al₂O₃ nanoparticles was successfully produced by compocasting technique followed by FSP. This fabrication route is suggested to be suitable for the production of other ceramic nanoparticles reinforced Al-based composites.

- The addition of 1wt% of Al_2O_3 nanoparticles has significantly reduced the grain size of both the cast and FSPed microstructures, leading to a grain size reduction from 28 μm to 18 μm in cast the cast condition and from 3.7 μm to 2.7 μm after FSP.
- The application of FSP to the unreinforced alloy induced a noticeable increase in hardness, tensile strength (+53%), yield strength (+25%) and ductility in comparison to the same cast material.
- In comparison to the as cast AA2024 alloy, UTS and YS of AA2024-1wt.% Al_2O_3 nanocomposite were enhanced by 71% and 30%, respectively, through FSP. The improvement was due to uniform distribution of Al_2O_3 reinforcement and grain refinement of aluminum matrix.
- AA2024- Al_2O_3 nanocomposite presented remarkably increased microhardness in comparison to the unreinforced alloy, both in the as cast and FSPed condition, at all the investigated depths. Such differences should be ascribed to the strengthening role exerted by nanoparticles and grain refinement induced by FSP.
- Compocasting technique and subsequent FSP was proved to be a promising method to treat casting defects in terms of porosity and shrinkage cavity and also to produce surface nanocomposites characterised by good dispersion of reinforcement and high levels of strength and ductility.

Acknowledgement.

This study was part of a research project on the development of nano-dispersed cast light aluminium for structural applications using the friction stir processing technique. The project was supported by Egyptian Ministry of Scientific Research mobility grant no. 12-12A1 and STDF grant no. 3926, no. 5304, and by the Italian Foreign Affairs Ministry mobility project Italy-Egypt EG13M05 (12-12A1). MMZA and MMES would like to thank Eng. Hagar Amin and Eng. Rana Gamal at SSMMR-CSE for their help in EBSD data acquisition.

References

1. Srivatsan TS, Al-Hajri M, Smith C, Petraroli M. The tensile response and fracture behavior of 2009 aluminum alloy metal matrix composite. *Mat. Sci. Eng. A* 2003; 346: 91–100.
2. Hashim J, Looney L, Hashmi MS. Metal matrix composites production by the stir casting method. *J. Mater. Process. Technol.* 1991; 92–93: 1–7.
3. Kumar K, Verma D, Kumar S. Processing and Tensile Testing of 2024 Al Matrix Composite Reinforced with Al_2O_3 Nano-Particles. In: 5th International & 26th All India Manufacturing Technology, Design and Research Conference, India 2014.
4. Ralph B, Yuen HC, Lee, WB. The processing of metal matrix composites – an overview. *J. Mater. Proc. Technol.* 1997; 63: 339–353.
5. Sajjadi SA, Ezatpour HR, Torabi Parizi M. Comparison of microstructure and mechanical properties of A356 aluminum alloy/ Al_2O_3 composites fabricated by stir and compo-casting processes. *Mater Design* 2012; 34: 106–111.
6. El-Mahallawi I, Shash AY, Eid Amer A. Nanoreinforced Cast Al-Si Alloys with Al_2O_3 , TiO_2 and ZrO_2 Nanoparticles. *Metals* 2015; 5: 802–821.
7. El Mahallawi I, Shash Y, Rashad RM, Abdelaziz MH, Mayer J, Schwed A. Hardness and wear behaviour of Semi-Solid Cast A390 Alloy Reinforced with Al_2O_3 and TiO_2 Nanoparticles. *Arab J Sci Eng.* 2014; 39: 5171–5184.
8. Zhou W, Xu ZM. Casting of SiC Reinforced Metal Matrix Composites. *J. Mater. Proc. Technol.* 1997; 63: 358–363.
9. Lee CJ, Huang JC, Hsieh PJ. Mg based nano-composites fabricated by friction stir processing. *Scripta Mater.* 2006; 54: 1415–1420.
10. Mishra RS, Mahoney MW. Friction Stir Processing: A New Grain Refinement Technique to Achieve High Strain Rate Superplasticity in Commercial Alloys. *Materials Science Forum* 2001, 357–359: 507–514.
11. Berbon PB, Bingel WH, Mishra RS, Bampton CC, Mahoney MW. Friction Stir Processing: A Tool to Homogenize Nanocomposite Aluminum Alloys. *Scripta Mater.* 2001; 44: 61–66.
12. Zahmatkesh B, Enayati MH, Karimzadeh F. Tribological and Microstructural Evaluation of Friction Stir Processed Al2024 Alloy. *Mater. Des.* 2010; 31: 4891–4896.
13. Ahmed MMZ, Refat M, El-Mahallawi I. Manufacturing of Nano-Surface AA7075 Composites By Friction Stir Processing. *Characterization of Minerals, Metals, and Materials, TMS2014*, 2014; John Wiley & Sons.

14. Sun N, Apelian D. Microstructural Modification of A206 Aluminum Via Friction Stir Processing. *Material Science Forum*, 2009; 618–619: 361–364.
15. Sun N, Apelian D. Friction Stir Processing of Aluminum Cast Alloys for High Performance Applications. *JOM*, 2011; 63(11).
16. Nakata K, Kima YG, Fujii H, Tsumura T; Komazaki T. Improvement of mechanical properties of aluminum die casting alloy by multi-pass friction stir processing. *Mater. Sci. Eng. A*. 2006; 437: 274–280.
17. Hashim FA, Salim RK, Khudair BH. Effect of Friction Stir Processing on (2024-T3) Aluminum Alloy. *Int. J. Innov. Res. Sci. Eng. Technol.* 2015; 4: 1822–1828.
18. Guo JF, Liu J, Sun CN, Maleksaeedi S, Bi G, Tan MJ, Wei J. Effects of nano- Al_2O_3 particle addition on grain structure evolution and mechanical behaviour of friction-stir-processed Al. *Mat SciEng A*. 2014; 602: 143-149.
19. Gandra J, Miranda R, VilaÃ§a P, Velhinho A, Teixeira JP. Functionally graded materials produced by friction stir processing. *J Mater Process Tech* 2011; 211(11): 1659-1668.
20. Gandra J, Miranda RM, VilaÃ§a P. Effect of overlapping direction in multipass friction stir processing. *Mat Sci Eng A*. 2011. 528: 5592-5599.
21. Gandra J, Vigarinho P, Pereira D, Miranda RM, Velhinho A, VilaÃ§a P. Wear characterization of functionally graded Al–SiC composite coatings produced by Friction Surfacing. *Mater Design*. 2013; 52: 373-383.
22. Ma SM, Zhang P, Ji G, Chen Z, Sun GA, Zhong SY, Ji V, Wang HW. Microstructure and mechanical properties of friction stir processed Al–Mg–Si alloys dispersion-strengthened by nanosized TiB_2 particles. *J Alloy Compd*. 2014; 616: 128-136.
23. Chen, Z, Li J, Borbely A, Ji G, Zhong SY, Wu Y, Wang ML, Wang HW. The effects of nanosized particles on microstructural evolution of an in-situ TiB_2 /6063Al composite produced by friction stir processing. *Mater Design*, 2015; 88: 999-1007.
24. Zhao Y, Kai X, Chen G, Lin W, Wang C. Effects of friction stir processing on the microstructure and superplasticity of in situ nano- ZrB_2 /2024Al composite. *Prog Nat Sci: Materials International*, 2016; 26(1): 69-77.
25. Yang R., Zhang Z, Zhao Y, Chen G, Guo Y, Liu M, Zhang J. Effect of multi-pass friction stir processing on microstructure and mechanical properties of Al3Ti/A356 composites. *Mater Charact*. 2015; 106: 62-69.

26. Eskandaria H, Taheria R, Khodabakhsh F. Friction-stir processing of an AA8026-TiB₂-Al₂O₃ hybrid nanocomposite: Microstructural developments and mechanical properties. *Mat SciEngA* 2016; 660:84-96.
27. Ahmed MMZ, Wynne BP, El-SayedSeleman MM, Rainforth WM. A comparison of crystallographic texture and grain structure development in aluminum generated by friction stir welding and high strain torsion. *Mater Design*, 2016. 103: 259-267.
28. Ahmed MMZ, Wynne BP, Rainforth WM, Threadgill PL. Microstructure, crystallographic texture and mechanical properties of friction stir welded AA2017A. *Mater Charact.* 2012; 64: 107-117.
29. Ahmed MMZ, Wynne BP, Rainforth WM, Threadgill PL. Quantifying crystallographic texture in the probe-dominated region of thick-section friction-stir-welded aluminium. *Scripta Mater.* 2008; 59(5): 507-510.
30. AhmedMMZ, Wynne BP, Rainforth WM, Threadgill PL. Through-thickness crystallographic texture of stationary shoulder friction stir welded aluminium. *Scripta Mater.* 2011; 64(1): 45-48.
31. Cury Camargo PH, Satyanarayana KG, Wypych F. Nanocomposites: Synthesis, Structure, Properties and New Application Opportunities. *Mat. Res.* 2009; 12 (1): 1–39.



Figure 1. Macrographs of AA2024-Al₂O₃ nanocomposite in the (a) as cast condition and (b) after FSP.

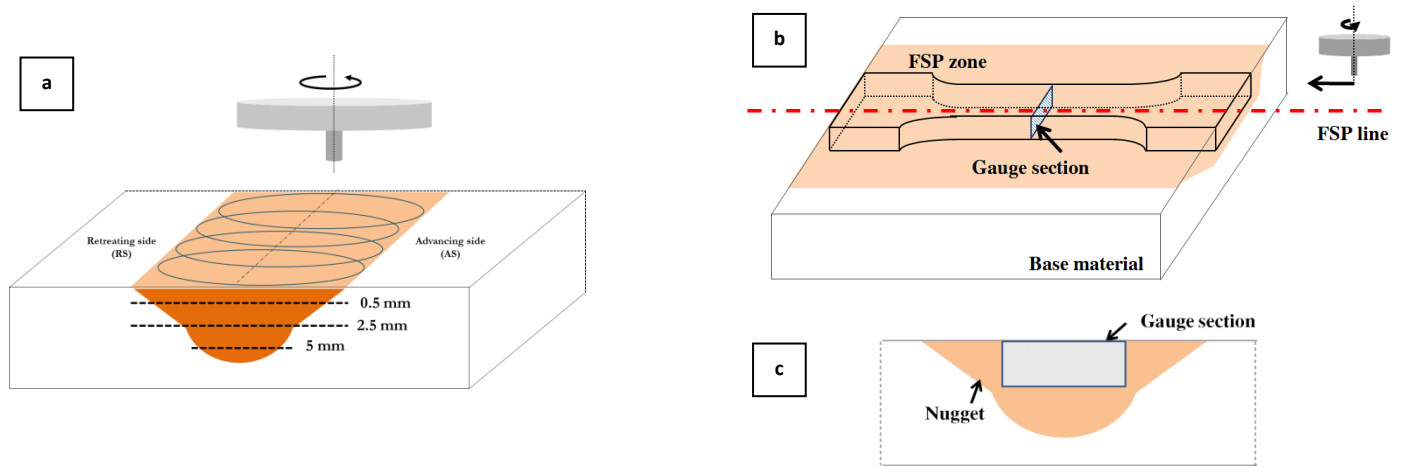


Figure 2. Schematic illustrations of (a) the position of microhardness profiles carried out on the samples cross section, (b) the extraction zone of tensile test specimens along the FSP line and (c) the position of the specimen gauge section within the nugget zone.

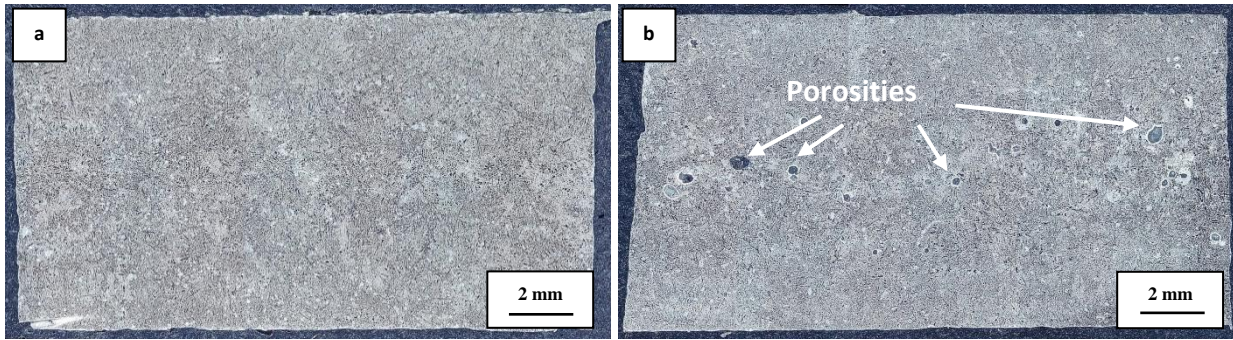


Figure 3. Multifocal images of the macrostructure of semi-solid processed (a) unreinforced AA2024 alloy and (b) AA2024-Al₂O₃ nanocomposite.

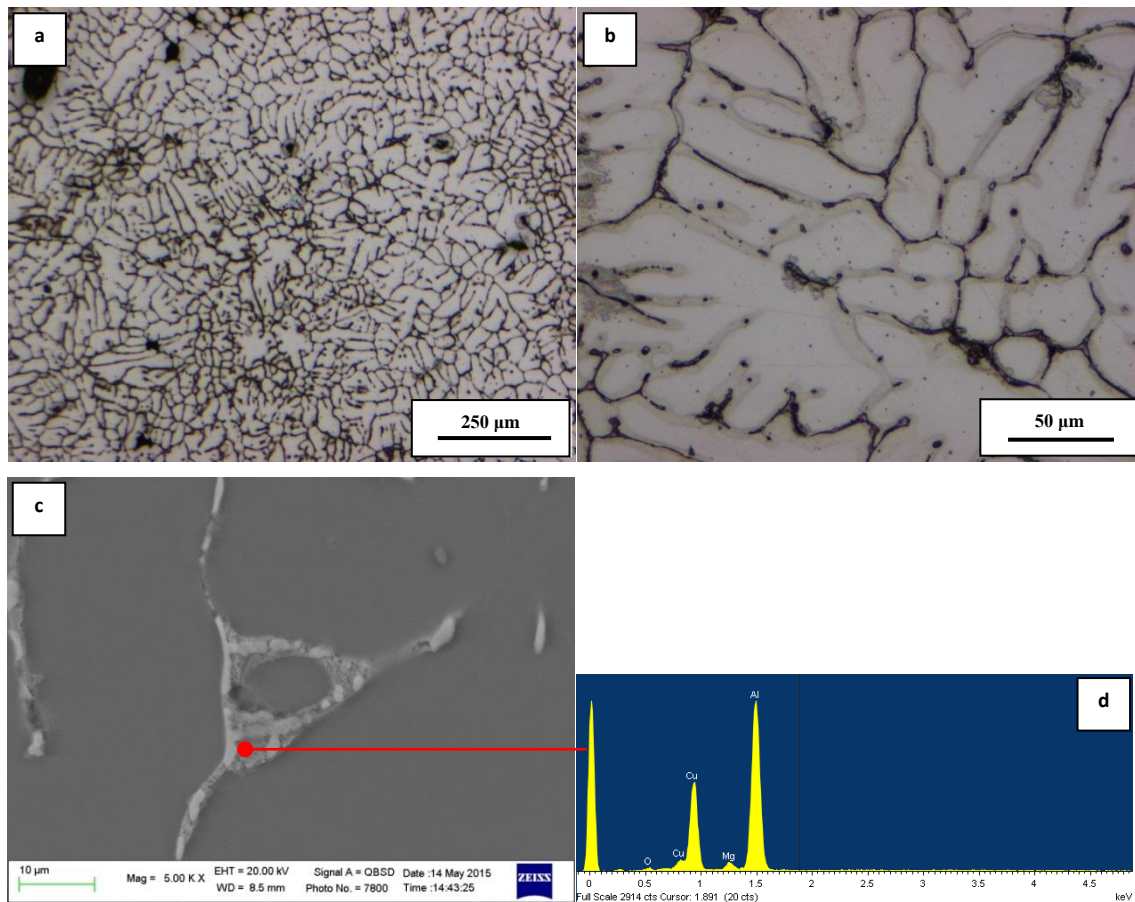


Figure 4. Optical images of the unreinforced AA2024 alloy in the as-cast condition at (a) low and (b) high magnification; (c) SEM image and (d) corresponding EDS spectrum of intermetallic compounds located in the interdendritic areas.

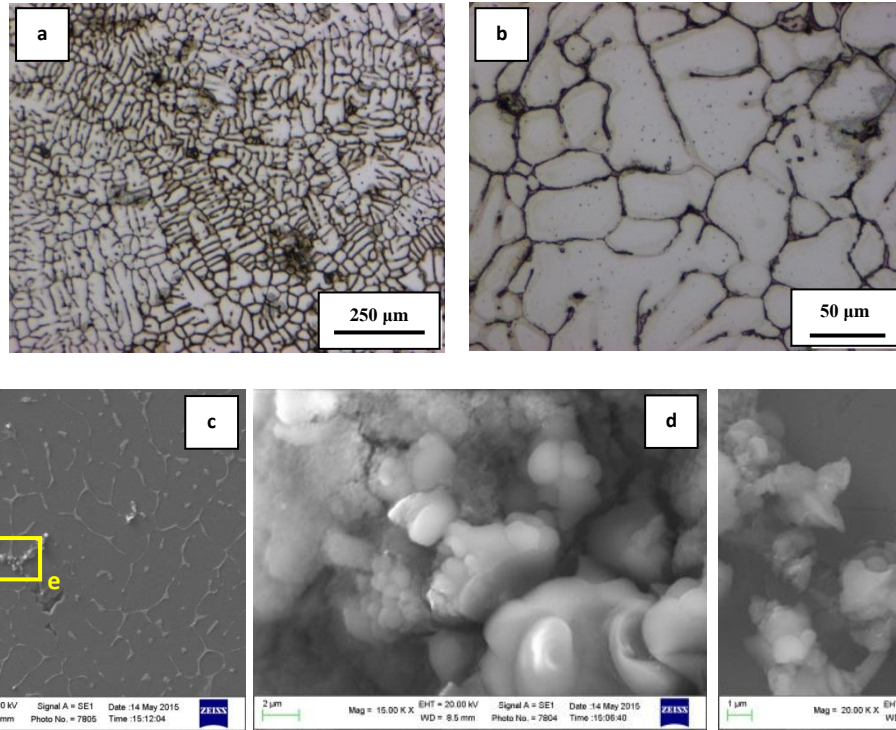


Figure 5. Optical images of AA2024- Al_2O_3 nanocomposite in the as-cast condition at (a) low and (b) high magnification; (c) SEM images of internal porosity associated with nanoparticles clusters, found both (d) at the pore boundaries and (e) in the interdendritic regions with corresponding EDS spectrum.

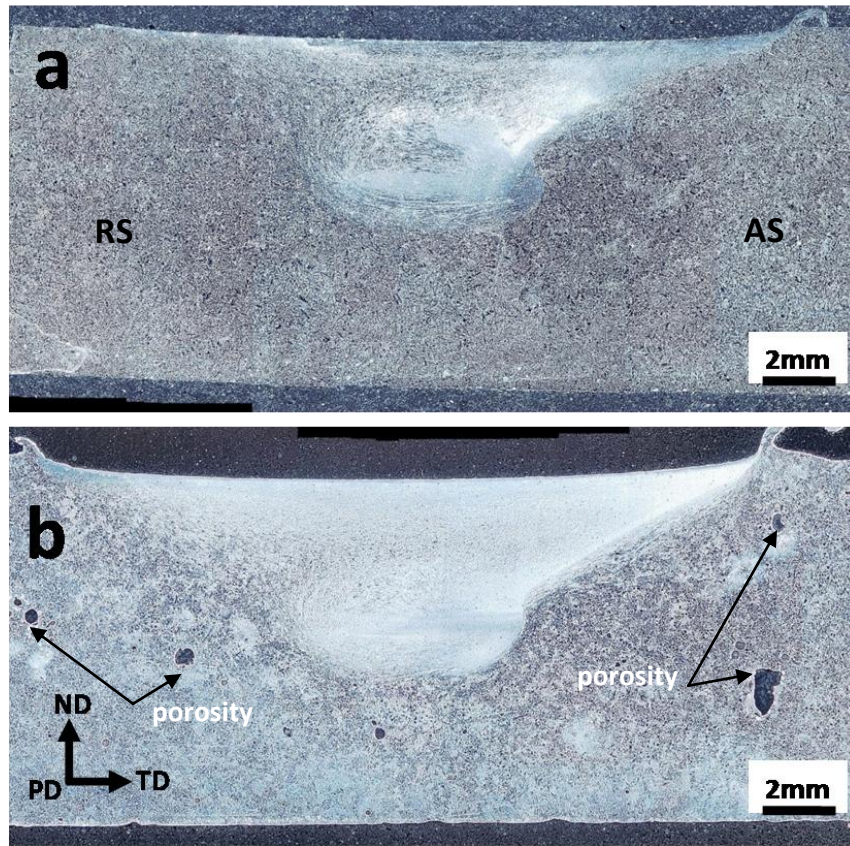


Figure 6. Multifocal macrographs of the transverse cross section of (a) FSP AA2024 alloy and (b) FSP AA2024-Al₂O₃ nanocomposite. TD is the transverse direction, PD is the processing direction and ND is the normal direction.

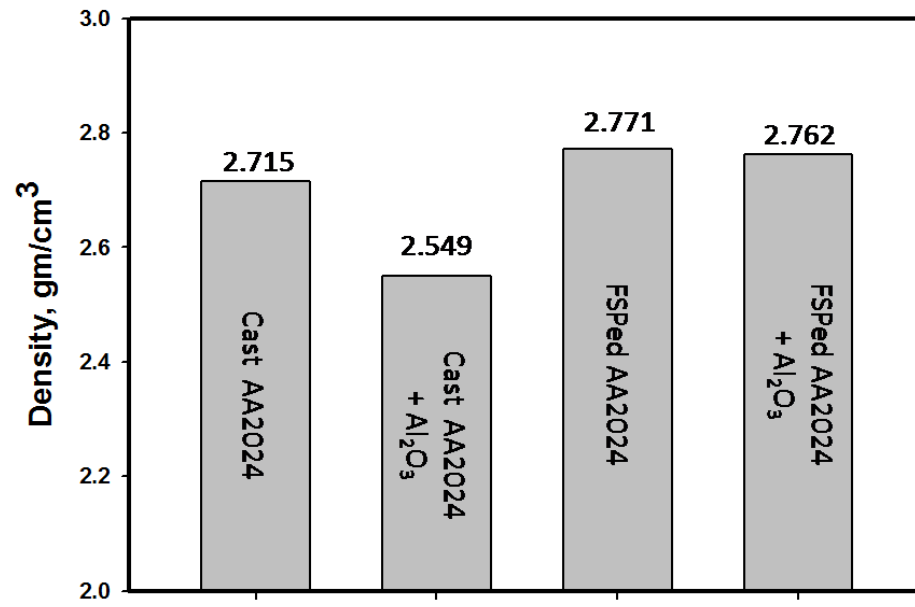


Figure 7. Average density of the investigated materials

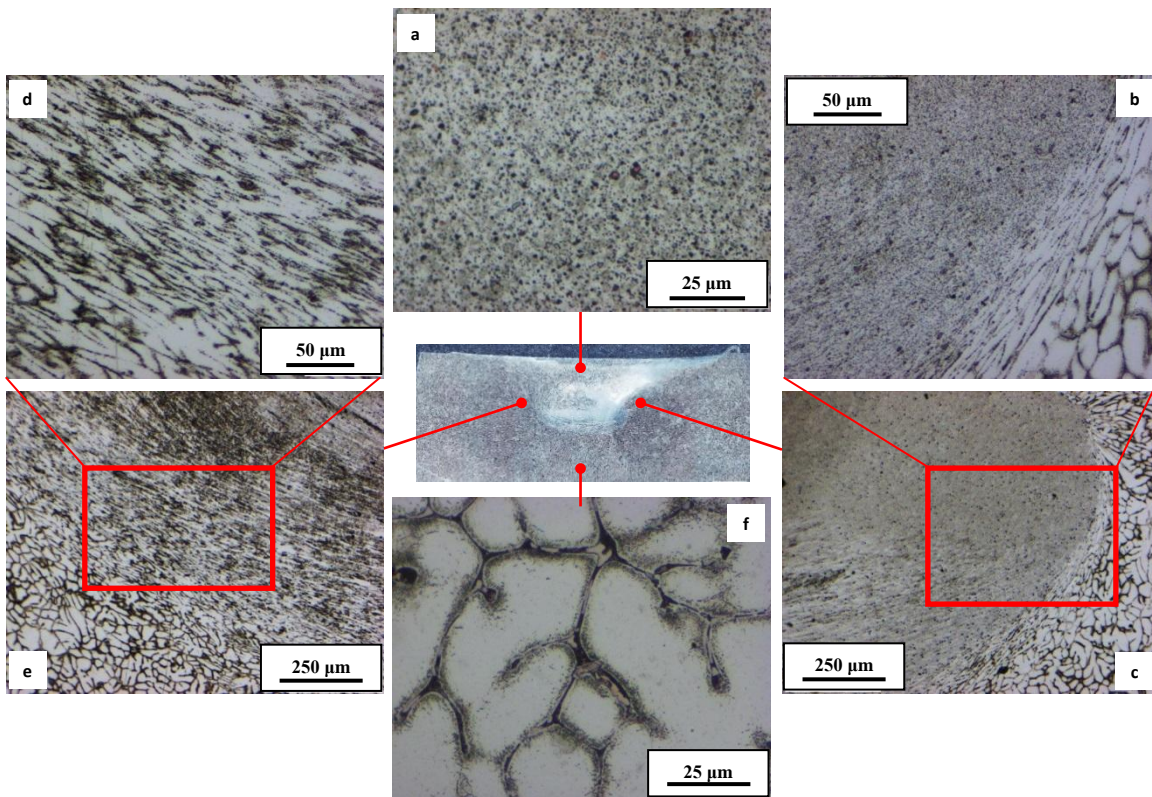


Figure 8. Optical images of FSP 2024 alloy showing the microstructure of (a) the nugget zone, (b,c) advancing side, (d,e) retreating side, (f) base material.

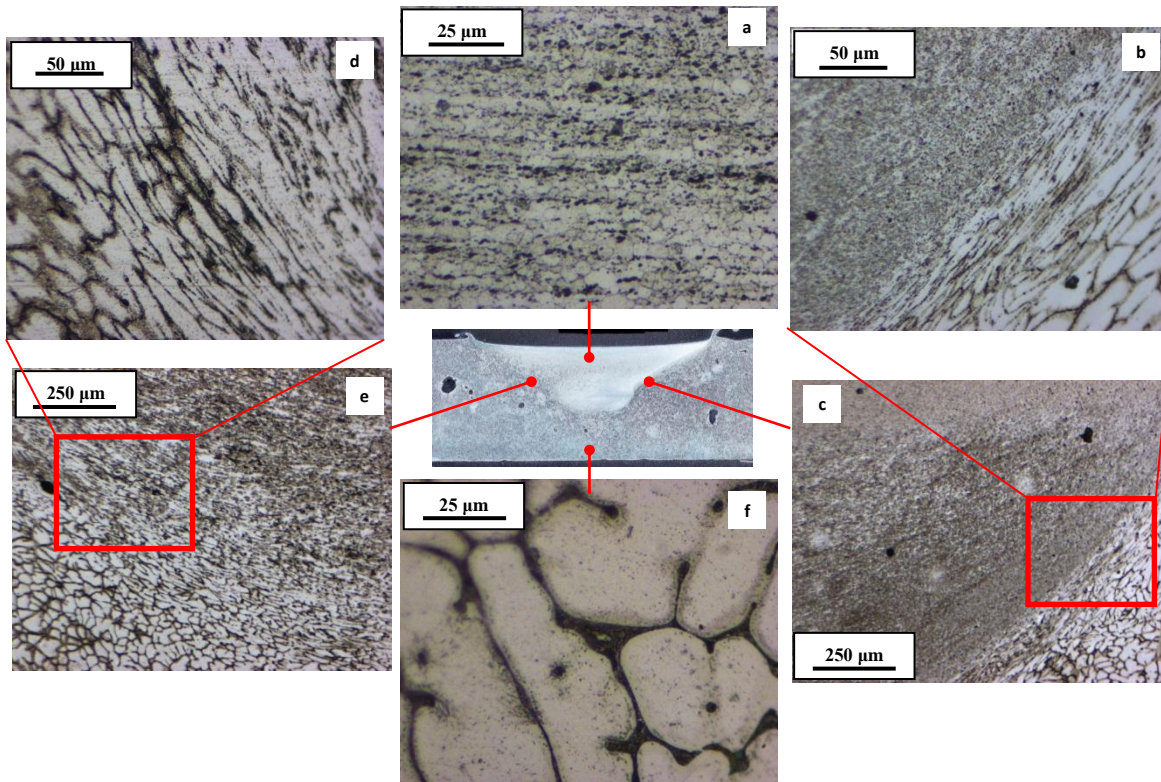


Figure 9. Optical images of FSP 2024-Al₂O₃ nanocomposite showing the microstructure of (a) the nugget zone, (b,c) advancing side, (d,e) retreating side, (f) base material.

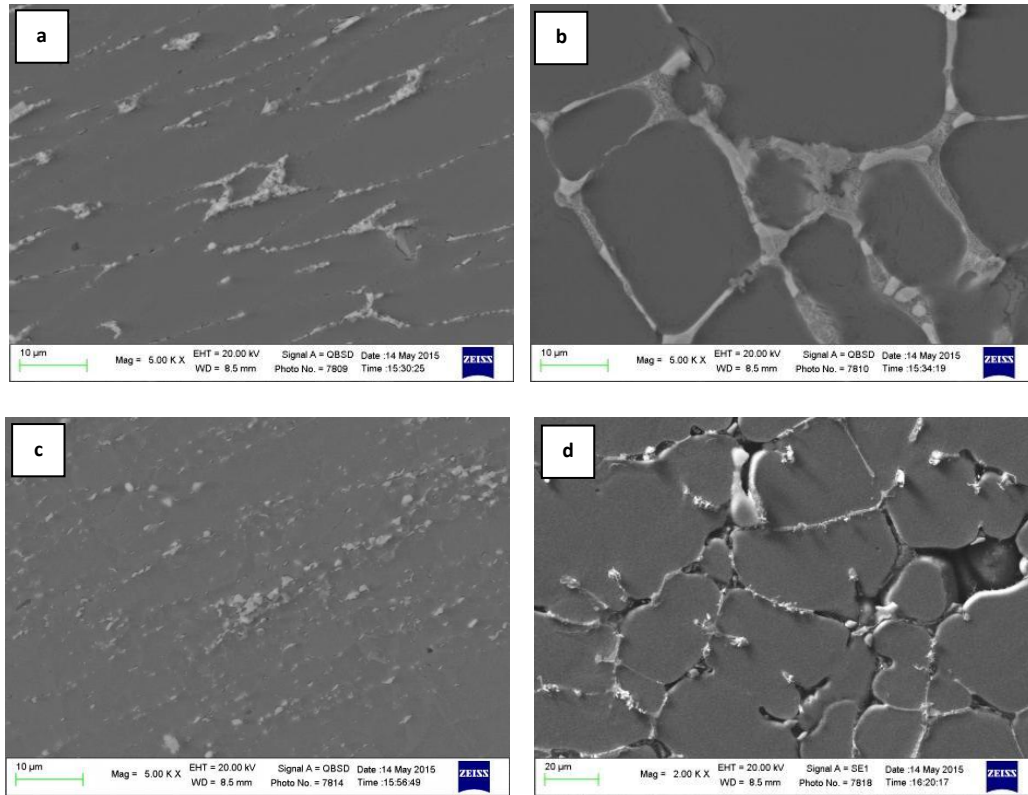


Figure 10. SEM images of (a) nugget zone and (b) base material of FSPed AA2024 alloy; (c) nugget zone and (d) base material of FSPed AA2024- Al_2O_3 nanocomposite, the latter containing nanoparticle clusters in the interdendritic regions, being unaffected by FSP.

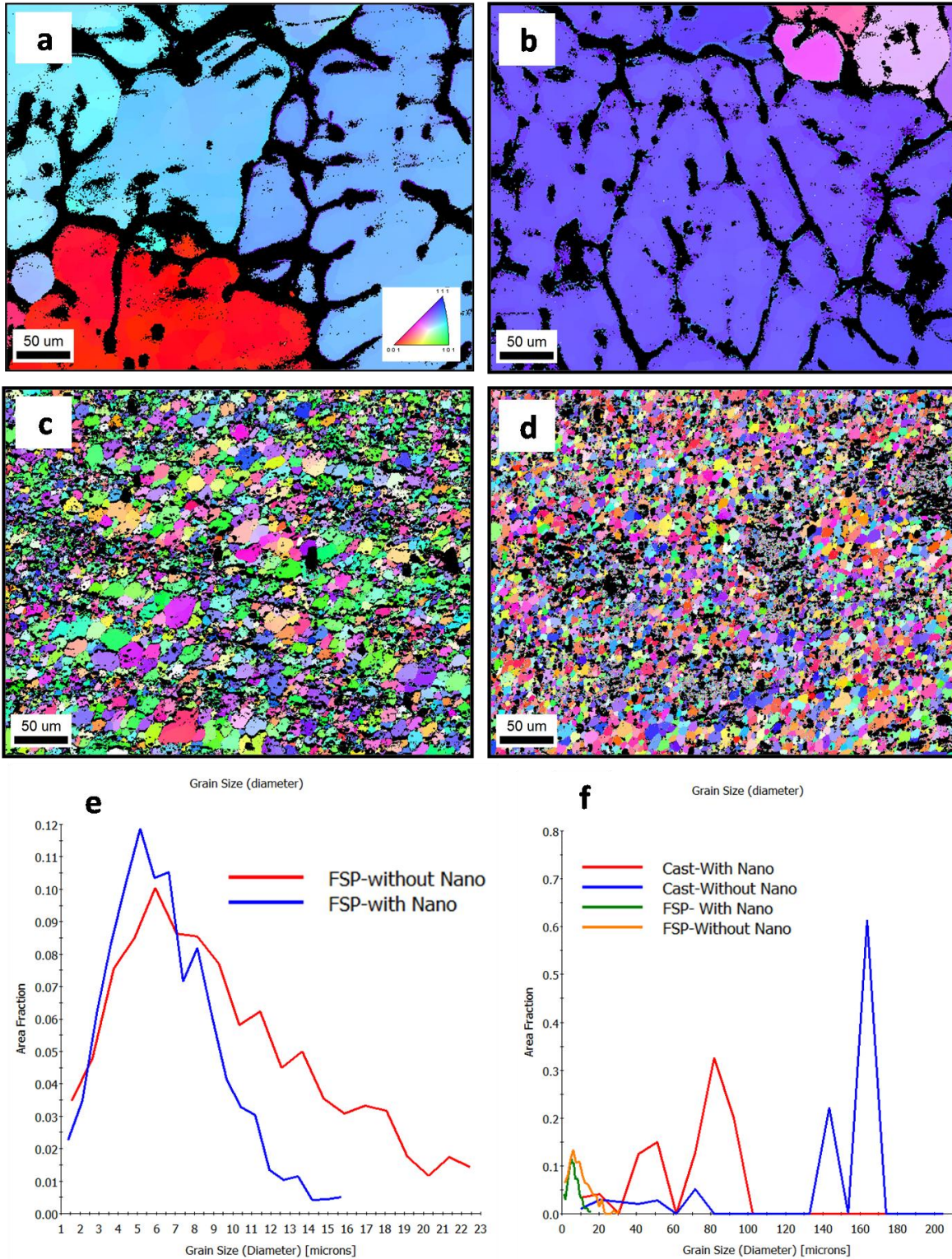


Figure 11. As obtained Orientation image maps in inverse pole figure colouring with respect to the FSP normal direction for (a) as cast unreinforced alloy, (b) as cast nanocomposite, (c) FSPed unreinforced alloy and (d) FSPed nanocomposite. (e) Grain size distribution of FSPed alloy and nanocomposite, (f) Grain size distribution of the cast and FSPed materials.

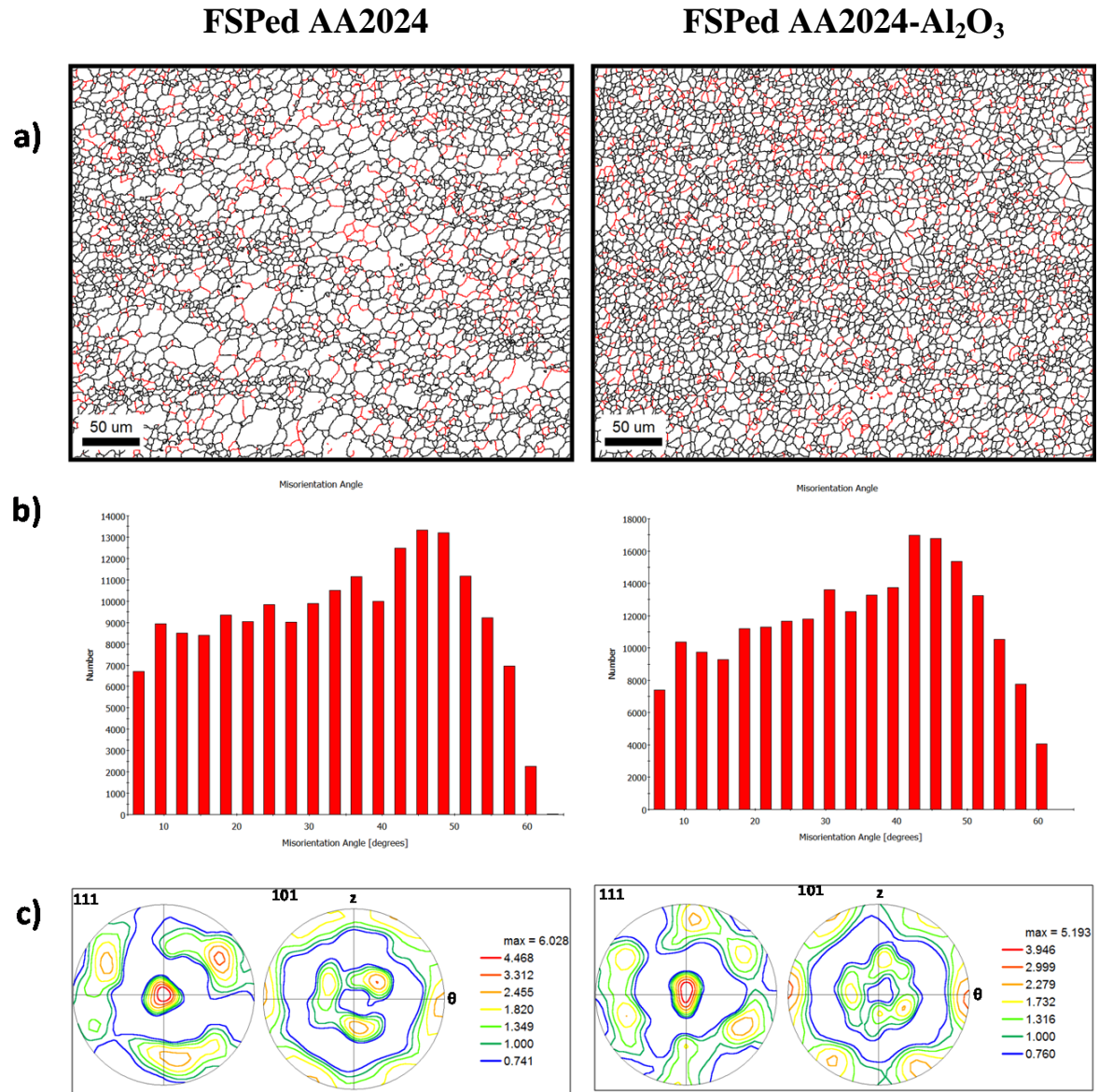


Figure 12. (a) Grain boundary maps with high angle boundaries $>15^\circ$ in black line and low angle boundaries $5-15^\circ$ in red line for the data sets presented in Fig. 11 after suitable treatment. (b) Misorientation angle distribution and (c) 111, 101 pole figures with respect to the standard shear reference axes (θ , z , r).

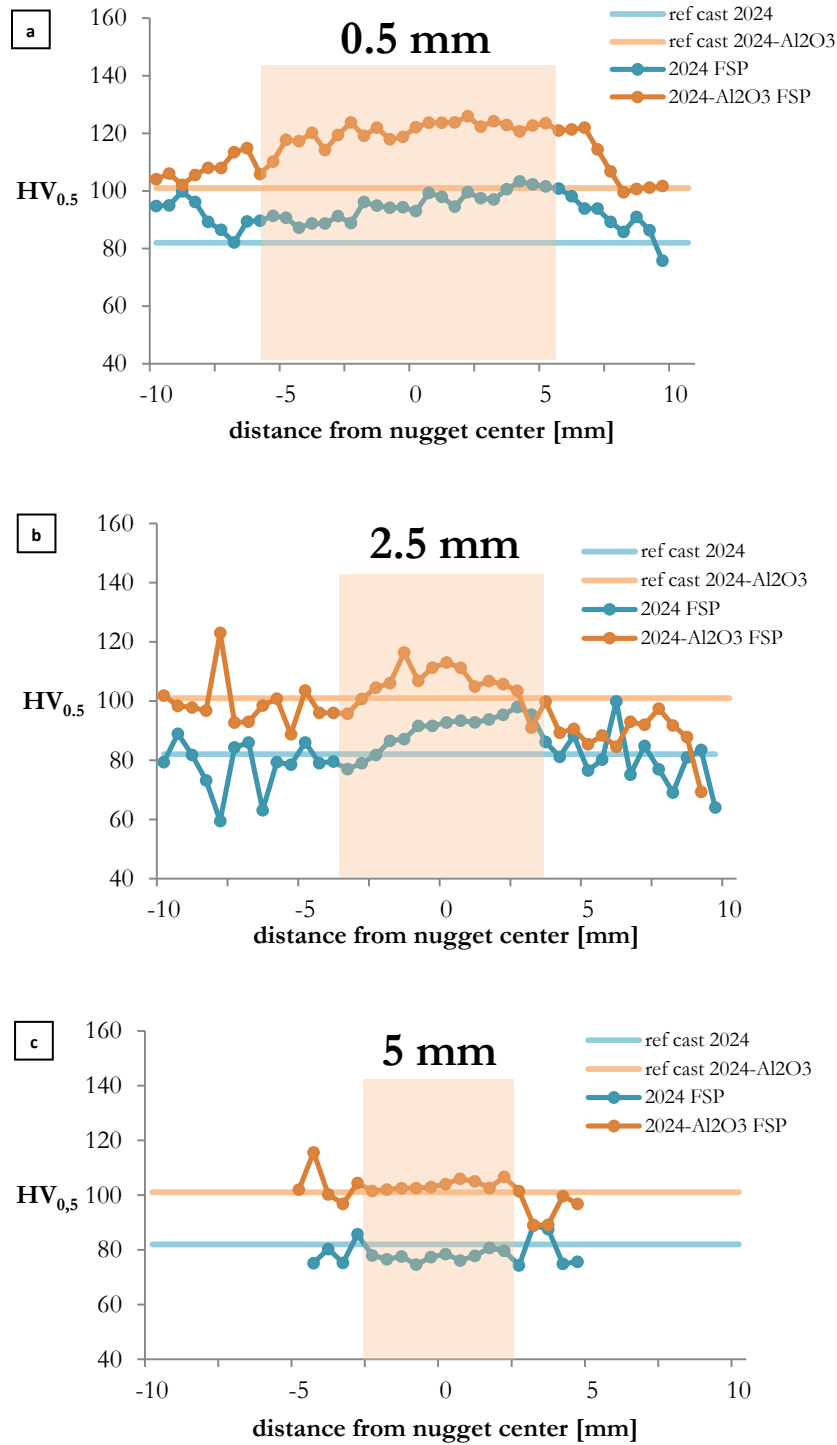


Figure 13. Vickers microhardness profiles of the unreinforced AA2024 alloy and AA2024-Al₂O₃ nanocomposite subjected to FSP; profiles were carried out at a depth of 0.5, 2.5 and 5 mm from the FSPed surface. The nugget position is indicated by the coloured area.

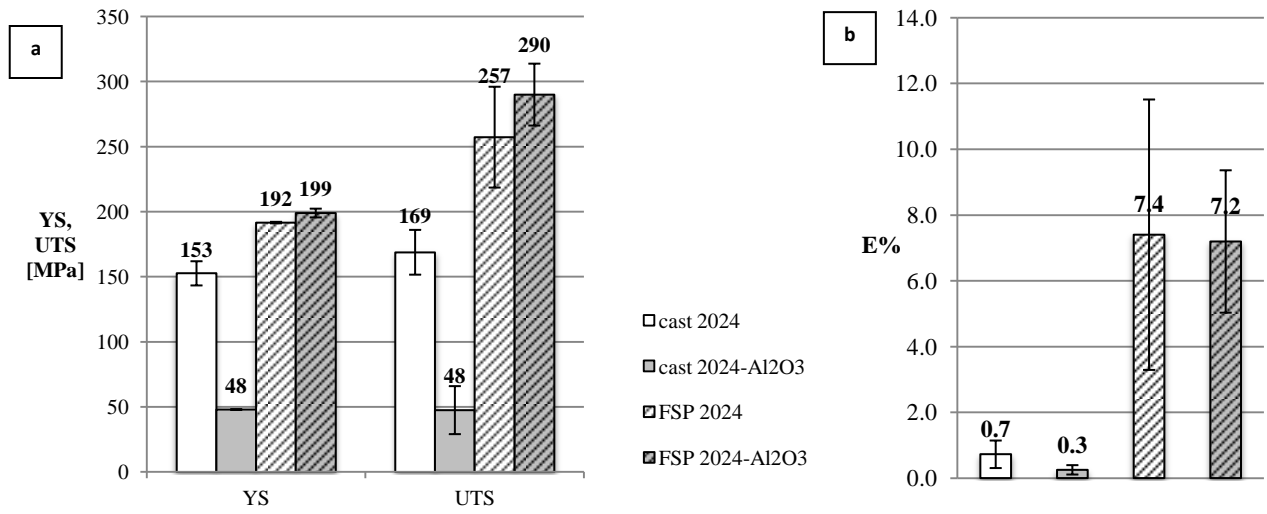


Figure 14. Tensile properties of the investigated materials: (a) Yield strength, YS, and Ultimate Tensile Strength, UTS, (b) elongation to failure, E%.

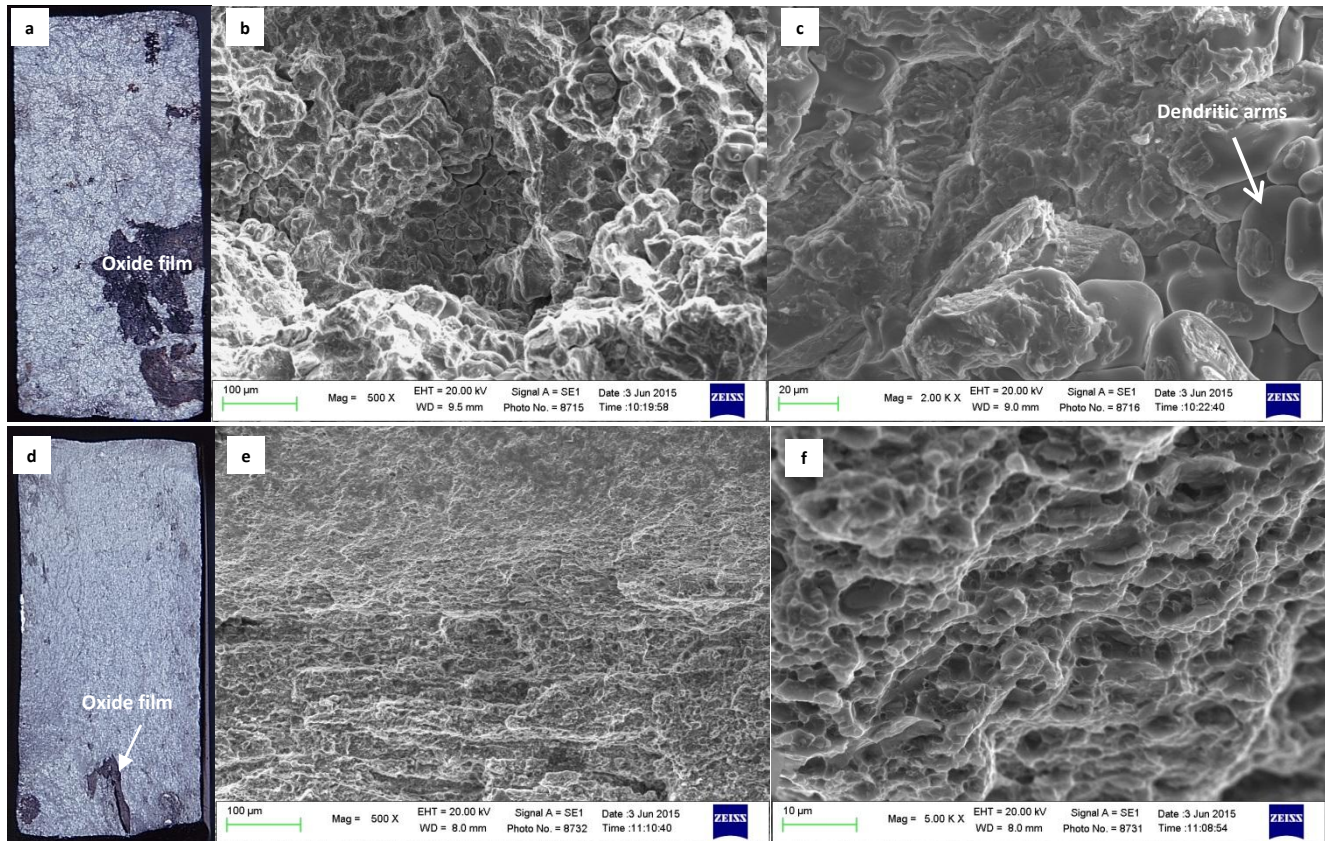


Figure 15. (a) Macrograph and (b, c) SEM images of as-cast AA2024 fracture surface, where oxides and dendritic arms associated to shrinkage cavities were observed. (d) Macrograph and (e, f) SEM images of FSPed AA2024 tensile fracture surface showing a typical ductile surface morphology, characterised by very small dimples and some oxides.

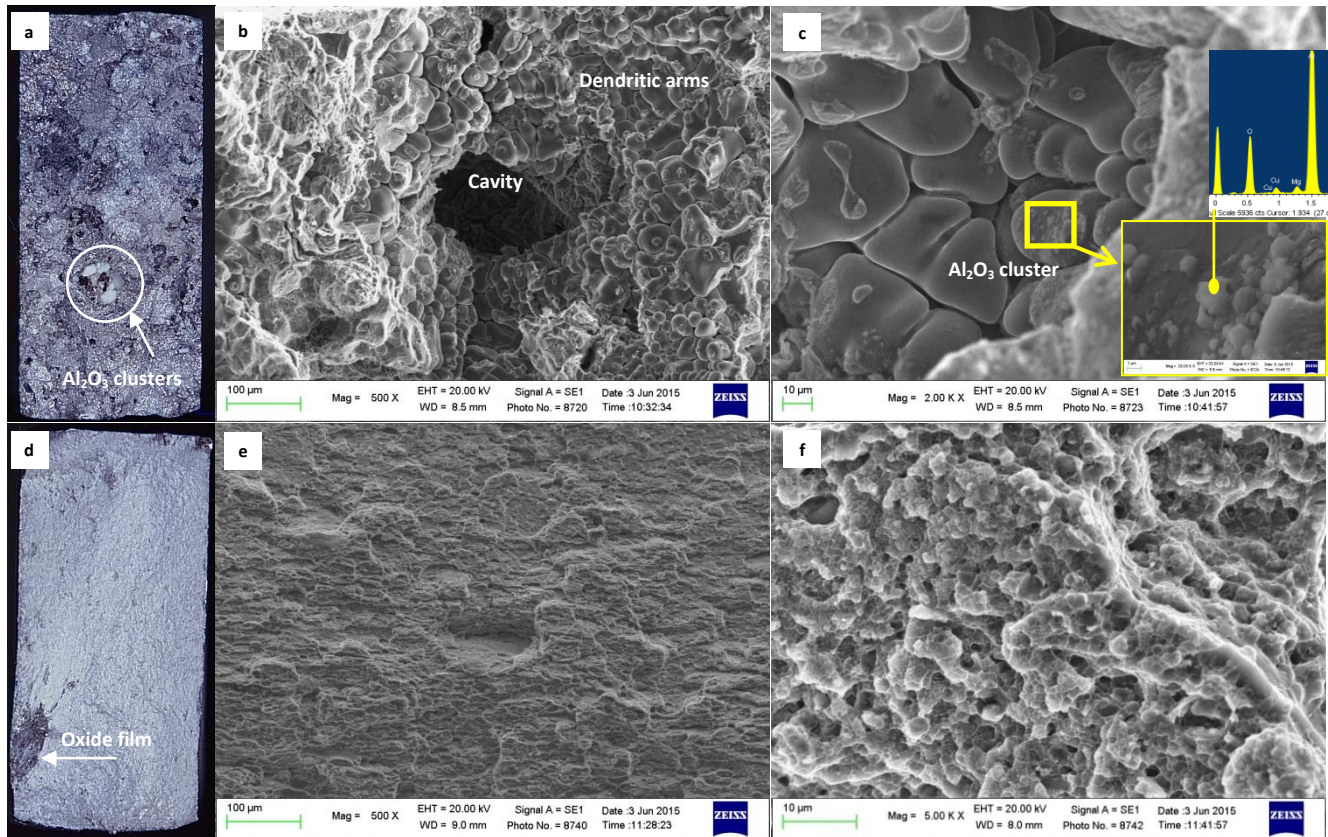


Figure 16. (a) Macrograph and (b, c) SEM images of as-cast AA2024-Al₂O₃ nanocomposite fracture surface showing oxides, dendritic arms associated to shrinkage cavities and nanoparticles clusters with corresponding EDS spectrum. (d) Macrograph and (e, f) SEM images of FSPed AA2024-Al₂O₃ nanocomposite tensile fracture surface; also in this case a typical ductile surface morphology with some oxides was observed.

Table 1. Chemical composition (wt %) of the AA2024 matrix

Element	Cu	Mg	Mn	Fe	Si	Zn	Cr	Al
wt%	4.39	1.26	0.57	0.50	0.50	0.25	0.10	Bal.

Table 2. Characteristics of the reinforcing Al₂O₃ nanoparticles.

Reinforcement	Density [g/cm ³]	Structure	E [GPa]	Average Size [nm]	Melting point [°C]
γ -Al ₂ O ₃	3.60	FCC	380	50	2054

Table 3. Materials and processing conditions investigated by tensile testing at room temperature.

Material	Process condition
AA2024	As cast
	After FSP
AA2024-Al ₂ O ₃	As cast
	After FSP